Supporting Information

for

Analyte-driven switching of DNA charge transport: *de novo* creation of electronic sensors for an early lung cancer biomarker

Jason M. Thomas, Banani Chakraborty, Dipankar Sen,* and Hua-Zhong Yu*

Department of Chemistry and Department of Molecular Biology and Biochemistry, Simon Fraser University, Burnaby, BC V5A 1S6, Canada

E-mail: sen@sfu.ca (D.S.); Hogan_yu@sfu.ca (H.Y.)

Materials and Methods:

General Biochemical Methods:

Oligonucleotides were synthesized by Integrated DNA Technologies and the University of Calgary DNA Core Services Lab; they were purified by denaturing PAGE (7M Urea/TBE), eluted by crush and soak into 10 mM Tris-HCl/0.1 mM EDTA, ethanol precipitated, and desalted by G-25 spin column. Oligonucleotide bioconjugates (5'-C6-disulfide-, 5'-anthraquinone, and 5'-ferrocene) were purified by HPLC: 250×4.6 mm Gemini 5 µm-C18 column (Phenomenex); solvent A: 0.1 M triethylammonium acetate (pH 7.0)/CH_3CN (20:1) and solvent B: CH_3CN; 20 minute linear gradient from 5% solvent B to 30% solvent B; flow rate of 1.0 mL/min. Oligonucleotides were 5'-^{32}P-labelled using T4 polynucleotide kinase (Invitrogen) and γ-^{32}P-ATP (Perkin Elmer) following the manufacturer's instructions, and PAGE purified as described above. Labelled oligonucleotides used in biochemical charge transfer assays were ethanol precipitated following the labelling reaction, resuspended in 10% aqueous piperidine, heated at 90 °C for 30 min, lyophilized extensively, then PAGE-purified as described above. Autoradiography imaging and quantification of gels were performed using a Typhoon 9410 phosphorimager with

ImageQuant v5.2 software. Quantitative data were plotted and fitted using Sigma Plot v10. For samples containing anthraquinone-conjugated oligonucleotides, exposure to ambient light was limited as much as possible. Note that the CLD binding buffer used throughout this study was 50 mM Tris-HCl (pH 8)/25 mM KCl/1 mM $MgCl_2$.

Cloning, Expression, and Purification of Recombinant CTAPIII and NAP2:

Both CTAPIII and NAP2 are produced *in vivo* by specific proteolytic cleavage of pro-platelet basic protein (PPBP) near its N-terminus.[s1] Therefore, CTAPIII and NAP2 gene inserts were prepared by PCR amplification using a commercially available plasmid template carrying the human PPBP gene (Gene Copoeia, cat. # HOC11892). The forward primers introduced both a 5'-NdeI restriction site (underlined) and a start codon (bold): CTAP-for: 5'-*AGCATGGTTCGAG*CAT**ATG**AACTTGGCGAAAGGCAAAG and NAP-for: 5'-*AGCATGGTTCGAG*CAT**ATG**GCTGAACTCCGCTGCATGTG. The reverse primer common to CTAPIII and NAP2 introduced a 3'-XhoI restriction site (underlined) directly downstream from the stop codon (bold): CTAP/NAP-rev: 5'-*ATCGTTCGGACAC*CTCGAG**CTA**ATCAGCAGATTCATCACCTG. The above primers included 13-nucleotide 5'-extensions (italics) to promote efficient restriction cleavage and ensure that the products could be easily resolved by agarose gel electrophoresis. PCR reactions to produce the CTAPIII and NAP2 inserts were run for 20 cycles: 45 sec at 95 °C, 45 sec at 50 °C, 60 sec at 72 °C. PCR products and cloning vector pET-21a were digested with NdeI and XhoI (Fermentas Fast Digest) and purified by agarose gel electrophoresis. Digested CTAPIII and NAP2 inserts were then ligated into the pET-21a vector and transformed into chemically competent BL21-de3 *E. coli* cells. Individual colonies were checked for the presence of the appropriately sized insert by colony PCR using vector-based outside primers (standard T7-promoter and T7-terminator primers). PCR products that contained a single insert were sequenced using the T7-promoter primer by the NAPS Unit (University of British Columbia).

The expression and purification protocol was adapted from that described for NAP2 by Malkowski *et al*.[s2] Transformant cultures were grown in LB (0.1 mg/mL ampicillin) at 37 °C to an optical density of 0.6-0.8. Expression was induced by the addition of β-IPTG to 1 mM, and was allowed to continue for 3.5 hours at 37 °C. Cells were harvested by centrifugation at 5000×g for

5 min at 4 °C. The resulting cell pellets were resuspended in strongly denaturing and reducing lysis buffer (6 M Guanidine-HCl/100 mM DTT/100 mM Tris-HCl (pH 8)/10 mM EDTA) and stirred at room temperature for 2 hours. Following lysis, the mixtures were centrifuged at 14,500×g for 15 min at 4 °C. The supernatant was acidified to pH 2 with trifluoroacetic acid and any precipitate formed was removed by brief centrifugation at 13,000×g. The acidified supernatants were applied directly to preparative reverse phase HPLC (home-packed, 1-inch diameter C-18; solvent A: 0.1% TFA in H_2O, solvent B: 90% CH_3CN/10% H_2O/0.1% TFA, 30 min linear gradient from 10% to 100% solvent B at a flow rate of 20 mL/min). The CTAPIII or NAP2 containing fractions were pooled, lyophilized, and resuspended at 2 mg/mL in oxidative refolding buffer: 2 M Guanidine-HCl/100 mM Tris-HCl (pH 8.6)/10 mM EDTA/2 mM oxidized glutathione/1 mM reduced glutathione. Following refolding for 2 hours at 37 °C, 10 to 20 mL samples were dialyzed twice against 4 L of 10 mM NaH_2PO_4 (pH 7.5)/150 mM NaCl, aliquoted and stored at -20 °C. Serial dilutions of CTAPIII for use in aptamer binding and CLD charge transfer experiments were prepared in 0.2 mg/mL BSA and 20 mM NaH_2PO_4 (pH 7.5).

Successful refolding was verified by comparing the reduced and refolded protein samples by ESI mass spectrometry, analytical reverse phase HPLC, and multimer crosslinking analysis. Analytical HPLC was performed using an Agilent Zorbax ODS RP-18 column at a flow rate of 1 mL/min using the solvent gradient described above. Protein concentrations were estimated from amino acid analysis, performed by the Advanced Protein Technology Center at the Toronto Hospital for Sick Children. Mass spectra were obtained by the Proteomics Core Facility in the Center for High Throughput Biology (University of British Columbia).

Crosslinking of CTAPIII and NAP2 Quaternary Structures:

CTAPIII and NAP2 were diluted to 0.2 mg/mL in 10 mM NaH_2PO_4 (pH 7.5)/10 mM NaCl. Crosslinking was initiated by the addition of 1/10th volume of 10 mM disuccinimidyl suberate (Pierce) in DMF and the reaction was continued for 30 minutes at room temperature. Reactions were terminated by the addition of 4 volumes of reducing SDS-PAGE loading buffer (Fermentas). Samples were heated to 100 °C for 5 min and analyzed by SDS-PAGE (Tris-Tricine buffer system[S3]) with silver staining.

Preparation of Anthraquinone Conjugated Oligonucleotide:

The anthraquinone conjugated oligonucleotide was prepared by reaction of the *N*-hydroxysuccinimidyl-ester of anthraquinone-2-carboxylic acid[s4] with the amino terminus of the AQ-oligo. This reaction was performed as described previously,[s5] with the exception that the conjugation reaction solvent was altered to a 1:1 mixture of DMF and 100 mM Na-borate buffer (pH 8.5). The anthraquinone bioconjugate was purified by HPLC as described above (Figure **S1**).

Results:

CTAPIII and NAP2 Expression:

Gene inserts for CTAPIII and NAP2 were prepared by PCR reaction using the pro-platelet basic protein gene as a template.[s1] These inserts were cloned into the pET-21a inducible expression vector and transformed into BL21-de3 *E. coli* cells. Protein expression, cell lysis under strongly denaturing and reducing conditions, reverse phase HPLC purification, and oxidative protein refolding were based on previously described procedures for NAP2.[s2] Analytical HPLC showed that CTAPIII and NAP2 were of very high purity and were cleanly refolded (Figures S2 and S3, respectively). Following refolding, the peaks corresponding to pure, reduced CTAPIII or NAP2 had completely disappeared and a single new peak appeared for each of oxidized CTAPIII or NAP2. The molecular masses of both the reduced and refolded samples were confirmed by mass spectrometric analysis (Figure S4 and S5). Mass spectra also showed that the initiating methionine was completely removed for NAP2, but was only partially removed for CTAPIII. Although the masses of both CTAPIII and NAP2 decreased slightly upon oxidative refolding, the expected loss of four hydrogen atoms could not be verified conclusively, as this small difference was beyond the precision of the mass spectrometer.

The quaternary structures of the refolded CTAPIII and NAP2 were investigated in order to verify successful oxidative refolding. Native CTAPIII and NAP2 are known to form tetramers and dimers, respectively, under low ionic strength conditions.[s6] Thus, multimers were trapped

at low ionic strength by covalent crosslinking with disuccinimidyl suberate and the products were analyzed by SDS-PAGE (Figure S6). Lanes 2 and 5 clearly demonstrate the formation of the crosslinked dimers and tetramers for refolded NAP2 and CTAPIII, respectively. In contrast, lanes 1 and 4 indicate a mixture of numerous multimers for the reduced (non-refolded) proteins. The crosslinking data, along with the clean conversion to a single oxidized state observed by HPLC, strongly suggest that both CTAPIII and NAP2 were successfully refolded to their native structures.

The purified, refolded CTAPIII and NAP2 were covalently linked to agarose beads to produce a solid phase immobilized target for aptamer selection. CTAPIII and NAP2 both display multiple lysine side chains on their solvent exposed surfaces,[s1] therefore, both were immobilized by reaction with NHS-ester activated agarose beads. This reaction appeared to be quantitative as the protein was completely consumed from the reaction supernatant as judged by SDS-PAGE analysis (Figure S7).

***In Vitro* Selection of CTAPIII-binding Aptamers:**

CTAPIII binding aptamers were isolated from a library of DNA oligonucleotides containing 40 degenerate positions using the *in vitro* selection procedure outlined in Figure S8.[s7] After brief washing with selection buffer, the sequences that remained bound to the solid phase-immobilized target were eluted and PCR amplified using an antisense primer that contained a single embedded ribose residue. Treatment of the PCR product with hot NaOH solution cleaved the antisense strand at the embedded ribose, which allowed the sense and antisense strands to be separated readily by preparative PAGE. Over the course of fifteen rounds of selection, the proportion of the input library that was observed to bind to the target increased slightly, but never progressed beyond ca. 5% (as judged by the fraction of the input radioactivity retained on the solid phase after washing). Nevertheless, the remaining library DNA was cloned and sequenced after the fifteenth round of selection.

The sequences of 26 clones were determined and aligned using the Clustal X program (Figure S9). Six aptamer sequence families are apparent in Figure S9, with the G-rich sequences of family F clearly dominating the final DNA pool. This suggested an explanation for the rather

low extent of target binding observed at the end of the selection: due to the high GC-content of the double stranded DNA pool (PCR products), standard denaturation conditions applied prior to gel loading had not adequately denatured the sense and antisense strands to allow for efficient separation by PAGE. Thus the DNA pool carried forward into each round of selection was significantly contaminated with the antisense strands. Not only do the anti-sense strands have no affinity for the selection target, but they also anneal to the sense strands preventing them from folding into functional aptamers. Reliable separation of the sense and antisense strands was achieved (following the SELEX experiment) by adding NaOH (to 50 mM) to the standard PAGE loading buffer, heating the samples at 100 °C, and snap cooling on ice before gel loading. Following this protocol, we isolated the pure aptamer (sense) strands from PCR products for representative aptamer clones from each family and for the round 15 DNA pool. Pull down assays were conducted with these aptamer samples to assess the binding of each to CTAPIII, NAP2, and the ethanolamine blocked agarose beads (Table S1). These data show that all of the selected aptamers bind to the protein target rather than the agarose beads, although affinity for the target is difficult to gauge due to the possibility of aptamer misfolding, exacerbated by the presence of the primer binding regions or other extraneous sequences.

Aptamer Characterization:

We first determined the boundaries of the functional aptamer domain within each full length clone sequence so that extraneous sequences could be removed. The intent was to incorporate an aptamer into a longer CLD oligo; therefore, we required functional aptamer domains of 40 to 50 nt or less, such that the resulting CLD oligo would be of a manageable length (i.e. < 80 nt). Aptamer domain boundaries were determined by randomly cleaving (at G and T residues) the full length aptamer sequence and determining which of the resulting fragments retained binding affinity for immobilized CTAPIII. This experiment was performed with both 5'- and 3'-^{32}P-labelled samples for at least one member of each sequence family. The data showed that the functional aptamer domains were significantly shorter than the full 80 nt clone sequence only for clone 27 (Family E) and clones 69 and 72 (Family F) (see Figures S10, S11, & S12). For all other clones tested, the functional aptamer domain required almost all of

the 80 nt sequences originally isolated from the selection (data not shown). Indeed, using secondary structure prediction as a guide, all attempts to truncate these clones to a reasonable length resulted in complete loss of CTAPIII binding activity. Thus only clones 27, 69, and 72 were retained for further investigation, as only these could be truncated to functional aptamer sequences short enough in length to make them practical for use in a CLD.

Besides the minimization of aptamer size, a crucial requirement for the creation of a successful CLD is aptamer conformational change upon target binding. We therefore carried out dimethylsulfate and $KMnO_4$ reactivity protection assays. Aptamer conformational changes can be detected by comparing the DNA damage patterns caused by these reagents in the absence and presence of the binding target. The data for clone 26 (same sequence family as clone 27) were especially promising in that several significant reactivity differences were noted in the presence of CTAPIII (Figure S13). Moreover, several CTAPIII dependent reactivity changes were clustered in the helical stem where the aptamer boundaries had been established. Therefore, this helical stem would likely be an ideal place to graft the aptamer onto the three-way helical junction of a CLD. In this way, changes in aptamer conformation upon CTAPIII binding would be proximal to the three-way junction and would likely have the most pronounced switching effect on its structure. Protection assays for clones 69 and 72 clearly establish the presence of G-quadruplex structures, as the addition of K^+-containing binding buffer led to characteristic decreases in guanine-N7 reactivity towards DMS for multiple guanine doublets and triplets (Figures S14 & S15). Although the protection patterns are dominated by K^+-dependent G-quadruplex formation, a few reactivity differences were noted upon CTAPIII binding for clones 69 and 72 that could suggest useful conformational changes. Overall, the protection data suggest that clones 69, 72, and especially 27 likely undergo conformational changes upon CTAPIII binding that could be practical in the context of a CLD.

Next, we evaluated the effect of aptamer truncation on CTAPIII binding affinity by native PAGE mobility shift assay. Three truncations of clone 27 were synthesized (Figure S16B) guided by the aptamer domain mapping data and secondary structure prediction. These truncations drastically improved the maximal extent of CTAPIII binding (Figure S16A), which suggests that the clone 27 aptamer is misfolded to a large extent in the case of the full 80 nt clone sequence.

The truncated aptamers 27-1, 27-2, and 27-3 showed similarly high CTAPIII affinities and extents of binding. The dissociation constant for aptamer 27-1 was determined more precisely by native gel shift to be 14 ±3 nM (Figure S17). Overall, the truncated helix appeared to provide an ideal starting point for designing and testing three-way junctions that connect the clone 27 aptamer domain to the CLD.

Two truncations for each of clones 69 and 72 were also assayed for CTAPIII binding activity (Figure S18). Complementary six nucleotide extensions were appended to the 5'- and 3'-ends of each of these truncated aptamers (69-1, 69-2, 72-1, 72-2) in an attempt to produce a helical attachment point ideal for CLD design. Binding affinity decreased substantially for aptamers 69-2 and 71-2, while aptamers 69-1 and 72-2 retained some affinity for CTAPIII. Although the latter could be useful in CLD construction, uncertainty about the G-quadruplex topologies posed possible structural complications in the attachment of these Family F aptamers to CLD three-way junctions. The conserved helical stem formed by the termini of the Family E aptamers presented a much more compelling choice for initial sensor design and testing.

Aptamer Incorporation into Coupled Ligand Deoxyribosensors and Biochemical Testing:

The functionality of CLDs was initially tested in biochemical assays, where charge transfer is initiated by excitation of a photo-oxidant anthraquinone appended to the reporter stem (Figure S19). Through-DNA charge transfer to photo-excited anthraquinone from the detector stem causes oxidative damage to the guanine triplet (denoted as "D" in Figures S19 & S20), which is monitored by piperidine-induced strand cleavage and PAGE analysis.

In light of the aptamer characterization data, which suggested that Family E aptamers possess properties desirable for sensor design/function, we began by testing CTAPIII CLDs incorporating the clone 27-1 aptamer with six different 3-way junction variations (Figure S20). Junction designs included those with two nucleotide bulges at either the 5'- or 3'- attachment points of the helical stem of the aptamer domain (constructs **S1**, **S2**, **S4**, **S5**, **S6**), as well as a design containing no unpaired nucleotides at the junction (construct **S3**). As shown in Figure

S20, the **S2** and particularly the **S3** sensor constructs showed increased charge transfer upon UV-irradiation in the presence of CTAPIII relative to a negative control in the absence of CTAPIII.

Electrochemical Testing of the Immobilized Coupled Ligand Deoxyribosensor for CTAPIII / NAP2:

The **S3** CLD was adapted for chip-based electrochemical detection of CTAPIII/ NAP2 by removing the guanine triplet from the detector stem, adding a 5'-hexane-thiol linker for immobilization on a gold surface, and replacing the 5'-tethered anthraquinone with ferrocene (a reversible 1-electron redox label). Figure S21 shows the oligonucleotide sequences and predicted secondary structure of the electrochemical **S3** CLD. The electrochemical behaviour of a ferrocene-terminated duplex DNA immobilized on a gold chip was also investigated. For relevant comparison with sensor **S3**, the sequence of this double helix was identical to that of the conduction path within the CLD.

Square wave voltammetry (SQW) was used to characterize changes in charge flow through CLDs in response to CTAPIII/NAP2 binding. Following preconditioning at positive potential to fully oxidize ferrocene (from Fe(II)) to (Fe(III)), a reduction sweep was used to quantify the electron transfer process. Figures 6 and 7 in the primary manuscript show the electrochemical response of the sensor **S3** and the duplex to CTAPIII/NAP2 binding. Figure S22 shows supplementary electrochemical data demonstrating little change in peak current for either sensor **S3** or duplex DNA upon addition of BSA to 100 nM (all experiments were performed in 50 mM Tris (pH 8.0)/25 mM KCl/1mM $MgCl_2$).

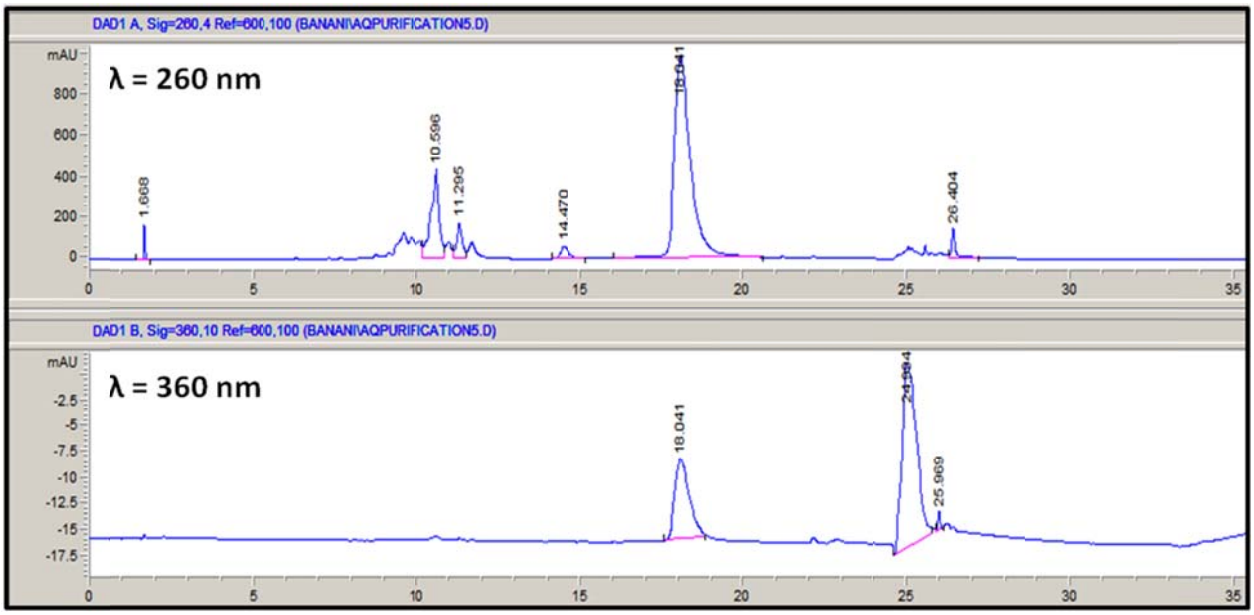

Figure S1: HPLC purification of anthraquinone-conjugated oligonucleotide. Chromatograms are shown for UV absorption detection at 260 nm (top trace) and 360 nm (bottom trace). The anthraquinone-conjugated oligonucleotide eluted at 18 min and was unique in that it absorbs strongly at both 260 nm and 360 nm.

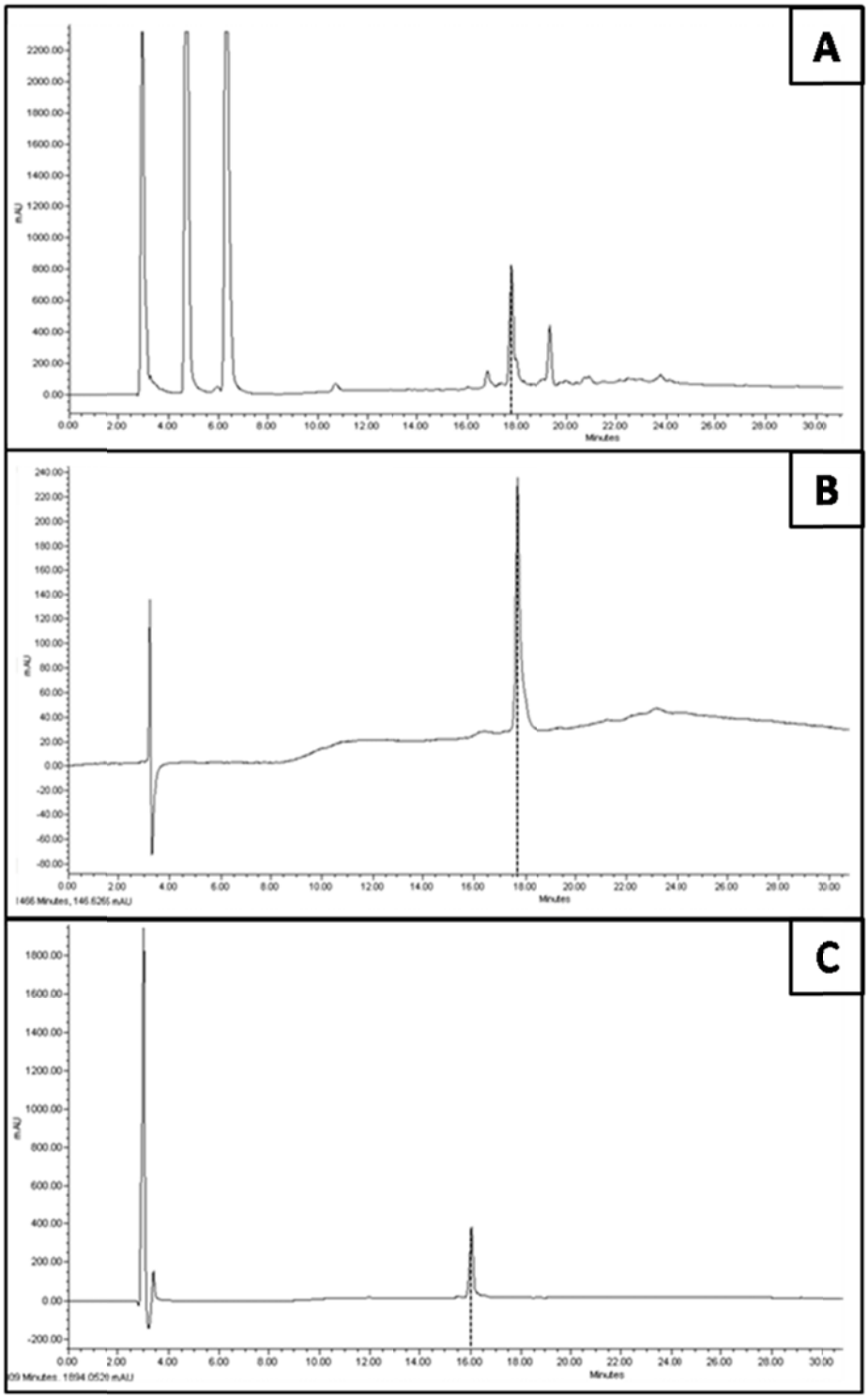

Figure S2: HPLC chromatograms (214 nm absorbance detection) showing the purification and refolding of recombinant CTAPIII. **(A)** Reduced (DTT), denatured (guanidine-HCl) crude cell lysate containing CTAPIII (retention time 17.7 min); **(B)** HPLC purified, reduced CTAPIII; **(C)** pure oxidatively refolded CTAPIII (retention time 16.0 min).

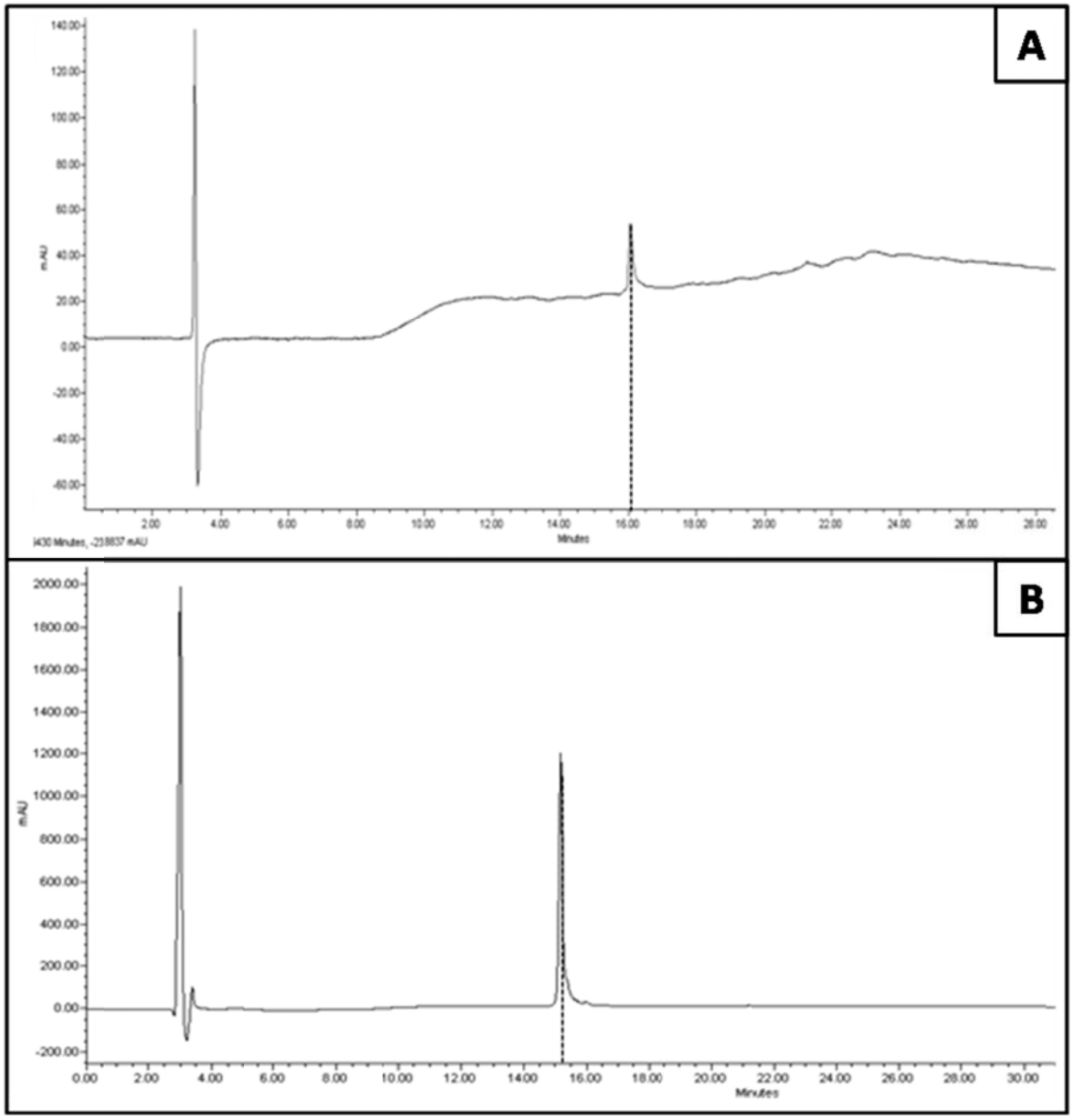

Figure S3: HPLC chromatograms (214 nm absorbance detection) showing the purification and refolding of recombinant NAP2. **(A)** HPLC purified, reduced NAP2 (retention time 16.1 min); **(B)** pure oxidatively refolded NAP2 (retention time 15.2 min).

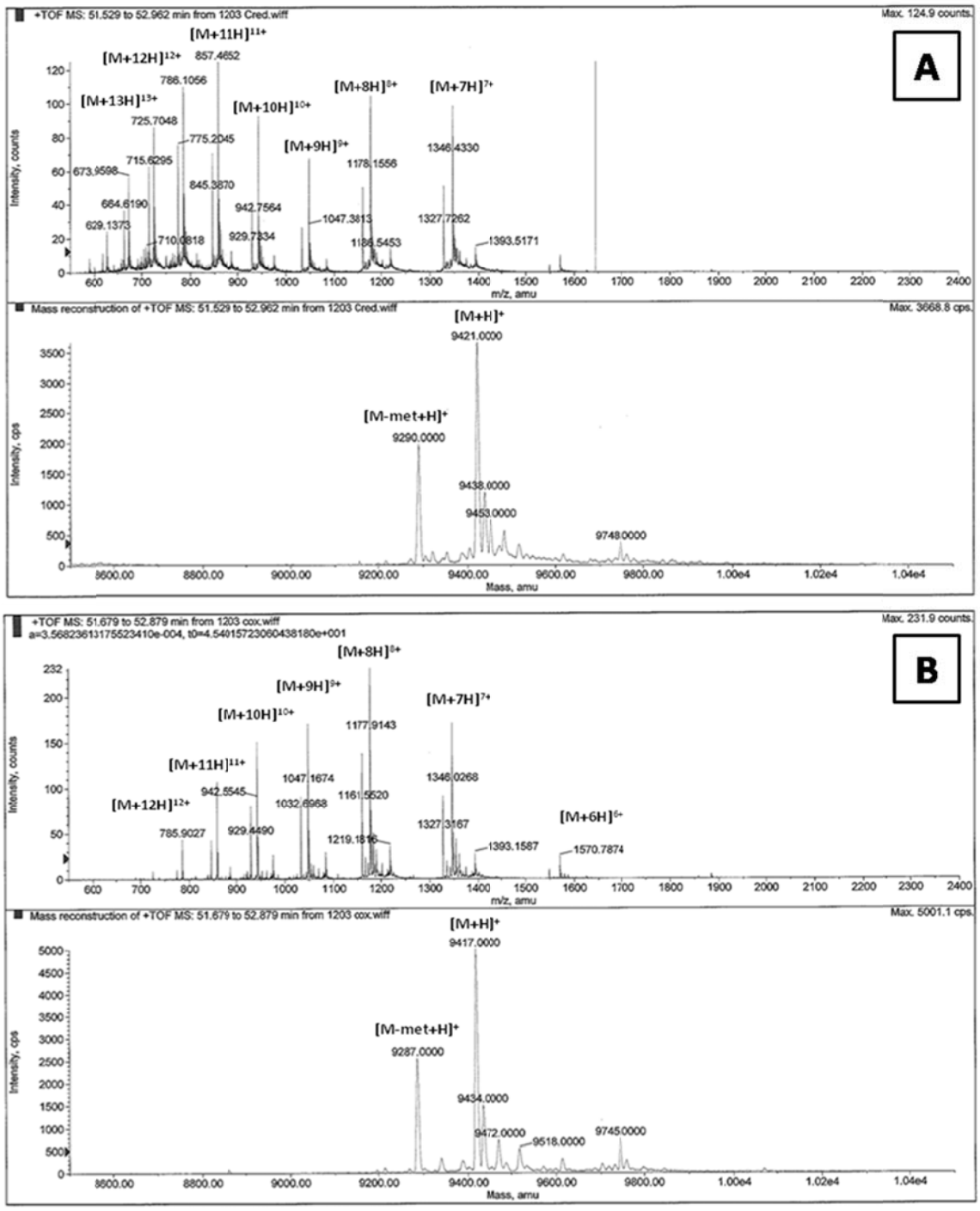

Figure S4: ESI mass spectra of recombinant CTAPIII. **(A)** HPLC purified, reduced CTAPIII. Average mass predicted = 9424.0, observed = 9421.0; demethionylated predicted = 9292.8, observed 9290.0. **(B)** Pure oxidatively refolded CTAPIII. Average mass predicted = 9420.0, observed = 9417.0; demethionylated predicted = 9288.7, observed 9287.0.

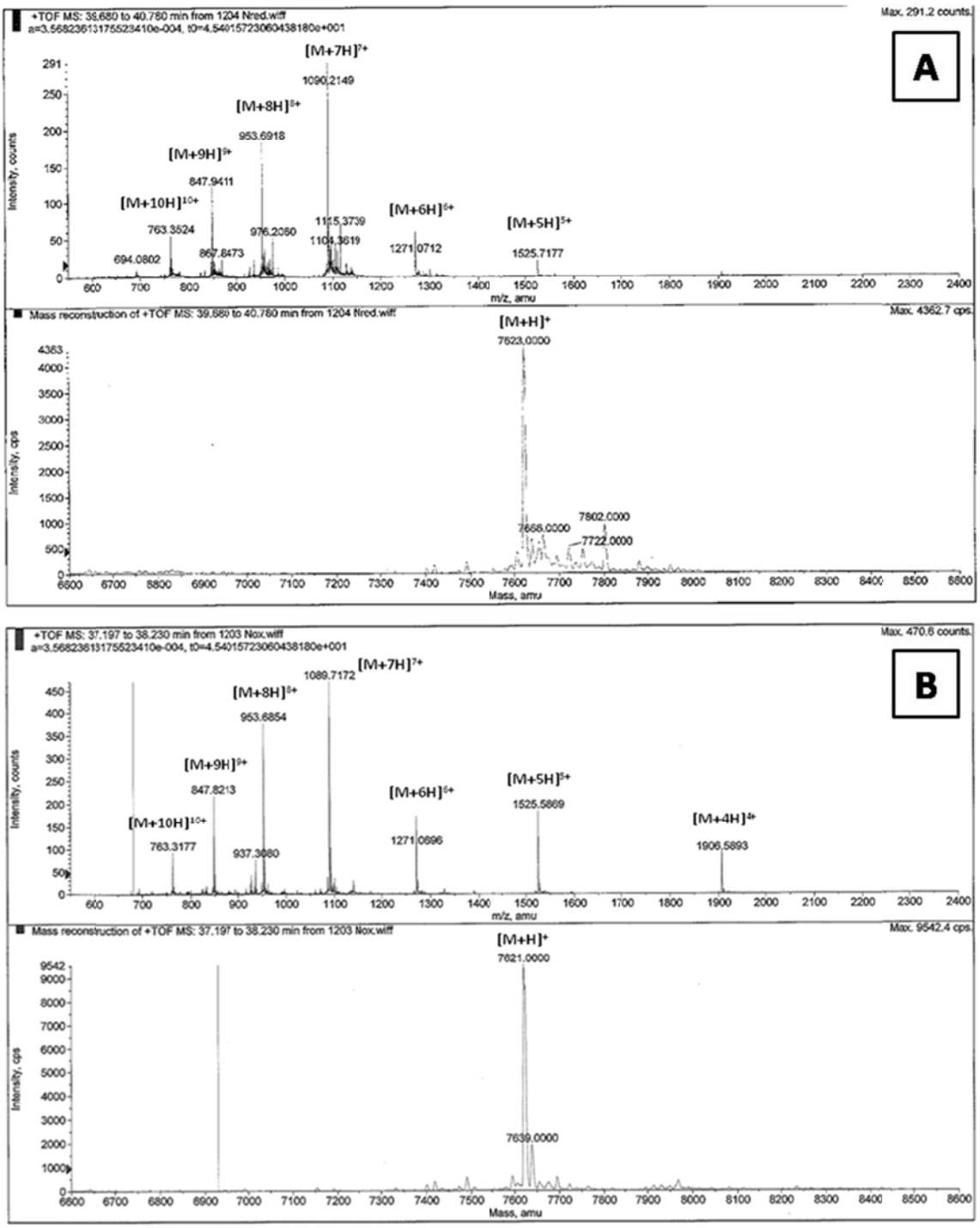

Figure S5: ESI mass spectral analysis of recombinant NAP2. **(A)** HPLC purified, reduced NAP2. Average demethionylated mass predicted = 7629.0, observed = 7623.0 **(B)** Pure oxidatively refolded NAP2. Average demethionylated mass predicted = 7625.0, observed = 7621.0.

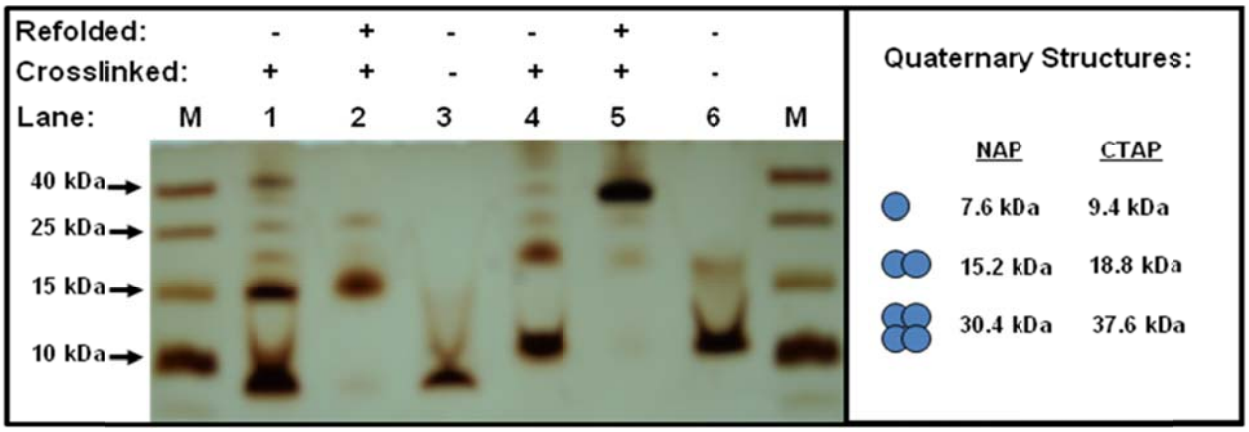

Figure S6: SDS-PAGE analysis with silver staining of recombinant CTAPIII and NAP2 following multimer crosslinking with disuccinimidyl suberate. Lane M = molecular weight markers; Lane 1: crosslinked reduced NAP2 (not refolded); Lane 2: crosslinked, refolded NAP2; Lane 3: reduced NAP2 (no crosslink); Lane 4: crosslinked reduced CTAPIII (not refolded); Lane 5: crosslinked, refolded CTAPIII; Lane 6: reduced CTAPIII (no crosslink).

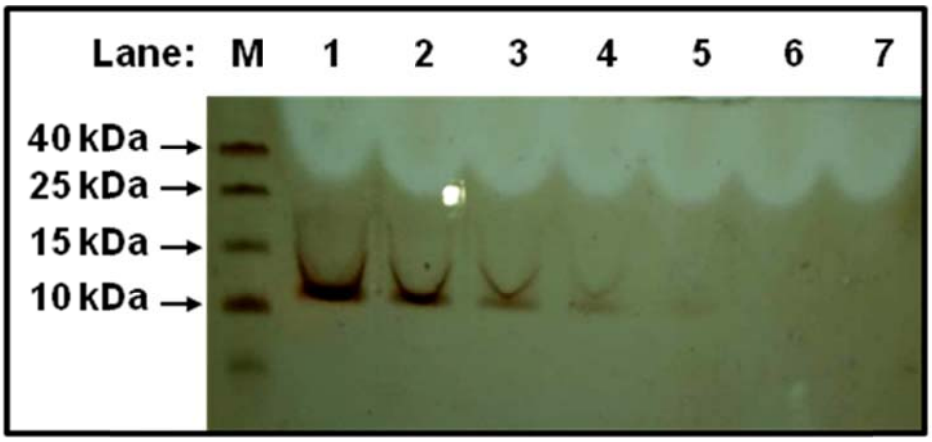

Figure S7: Analysis of the progress of solid phase immobilization of CTAPIII. Supernatant from the CTAPIII immobilization reaction was analyzed by SDS-PAGE at 0 min (Lane 1), 5 min (Lane 2), 10 min (Lane 3), 15 min (Lane 4), 20 min (Lane 5), 30 min (Lane 6), 40 min (Lane 7).

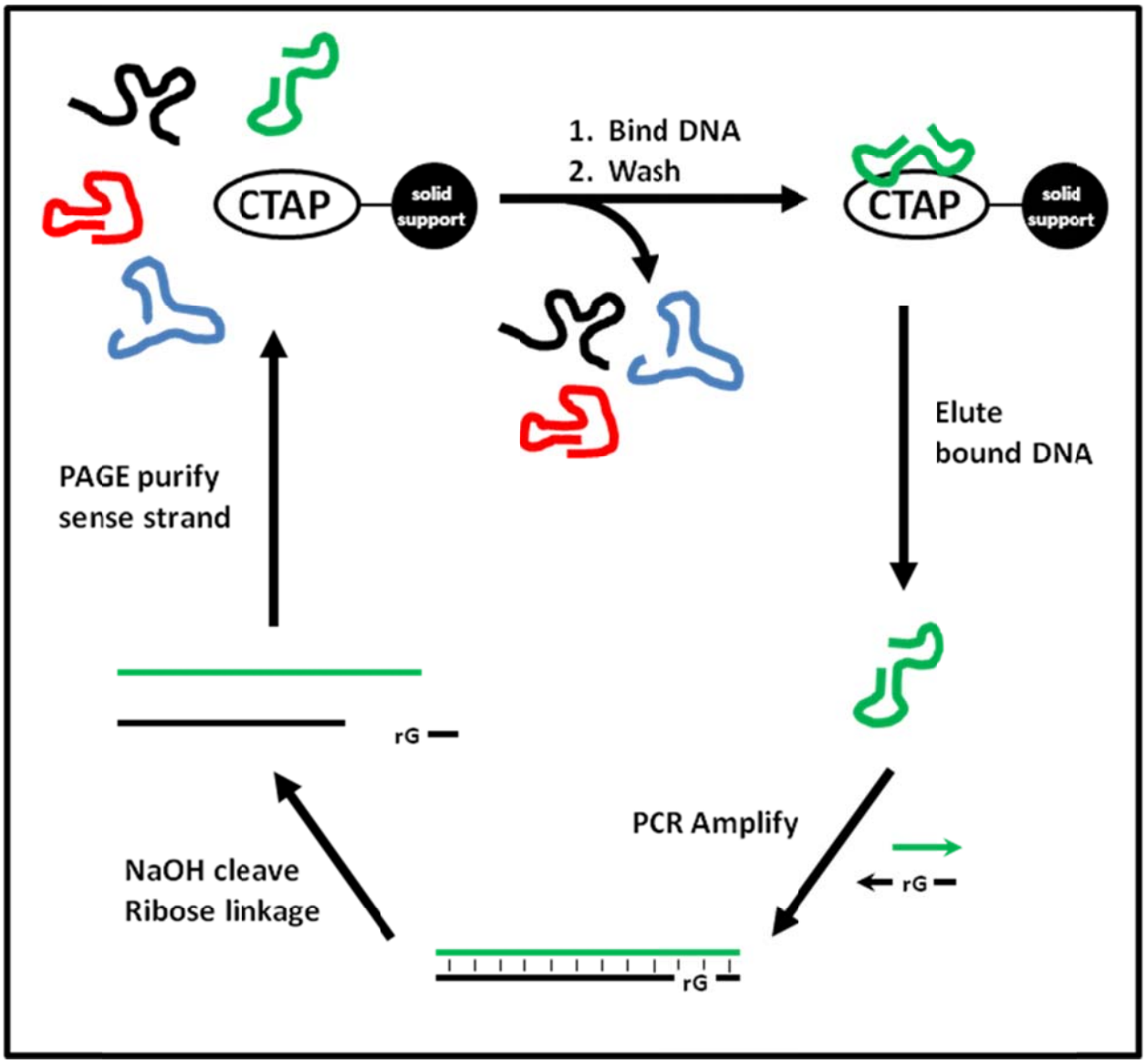

Figure S8: Outline of the SELEX procedure used to isolate CTAPIII binding DNA aptamers. rG = embedded riboguanosine.

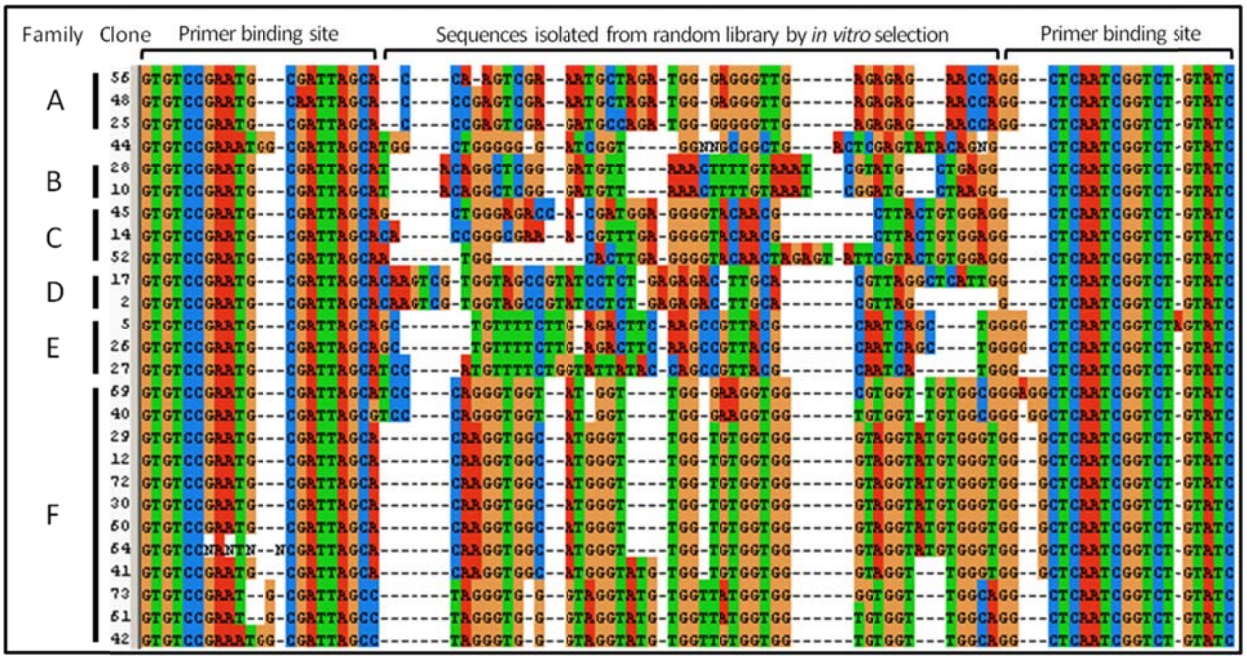

Figure S9: Sequences determined following cloning of the DNA pool that remained following 15 rounds of selection for CTAPIII binding. Sequences were aligned using Clustal X.

Clone #	CTAPIII Beads % Bound	NAP2 Beads % Bound	Blocked Beads % Bound
2	25	24	0.7
17	50	38	0.7
26	6	6	0.5
27	9	11	0.8
28	14	17	0.3
41	22	22	4.7
45	11	13	0.3
48	6	6	1.0
56	16	20	0.6
69	32	13	1.0
72	22	24	0.5
73	24	25	0.3

Table S1: Pull down bead binding assays, quantified by scintillation counting, comparing the binding of aptamer clones to CTAPIII or NAP2 conjugated agarose beads, and ethanolamine blocked agarose beads.

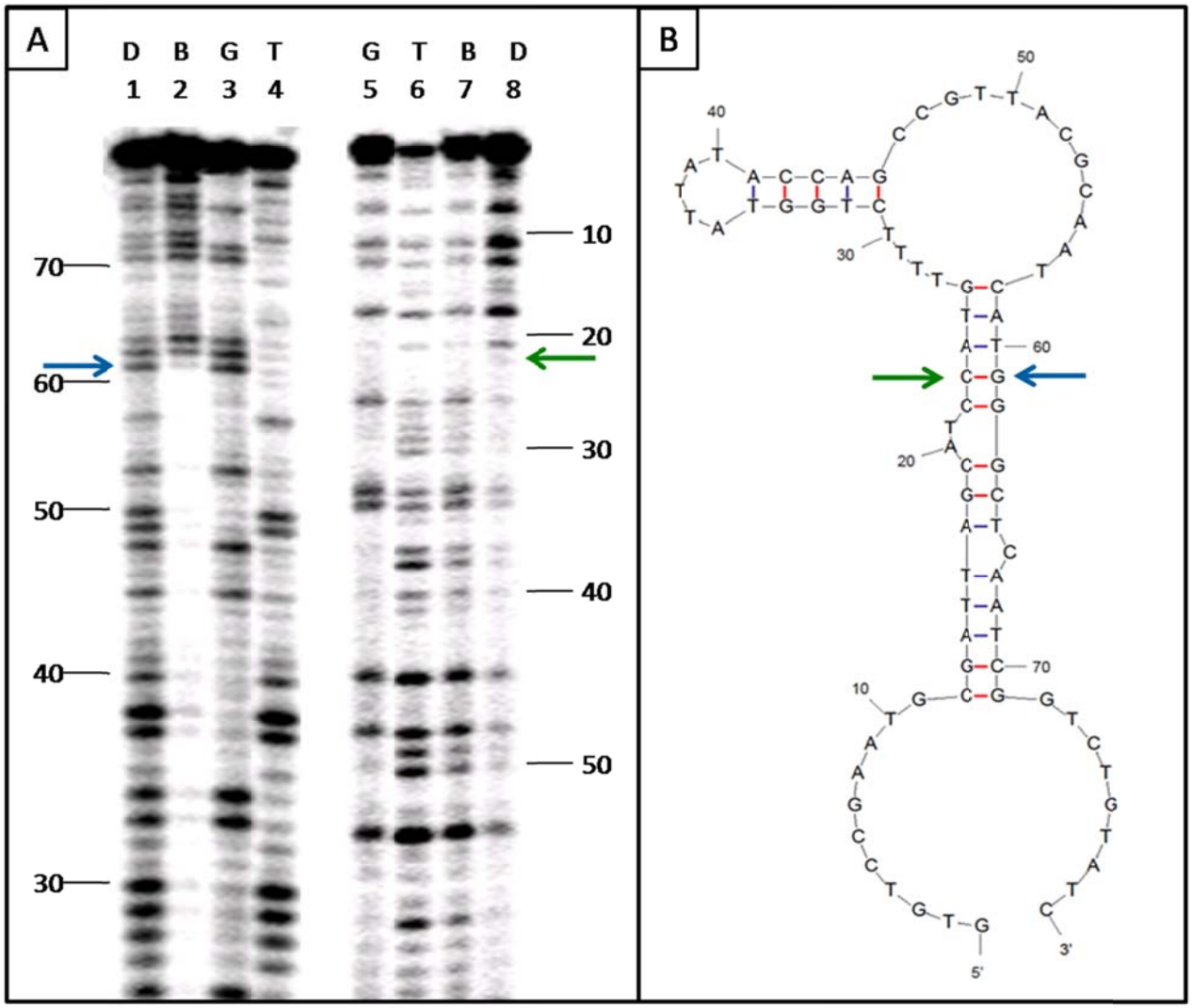

Figure S10: (A) Fragment binding experiments to map the boundaries of the clone 27 aptamer domain. Lanes G: G-specific cleavage ladder; lanes T: T-specific cleavage ladder; lanes B: mixture of G- and T-specific cleavage fragments that remained bound to CTAPIII beads after washing; lanes D: unbound fragments decanted and washed from CTAPIII beads. Lanes 1-4: 5'-labelled fragments; lanes 5-8: 3'-labelled fragments. Fragments were resolved by 12% PAGE. **(B)** Lowest energy secondary structure predicted by Mfold. The blue and green arrows denote the first required nucleotide at the 3'- and 5'-ends, respectively, of the core aptamer domain.

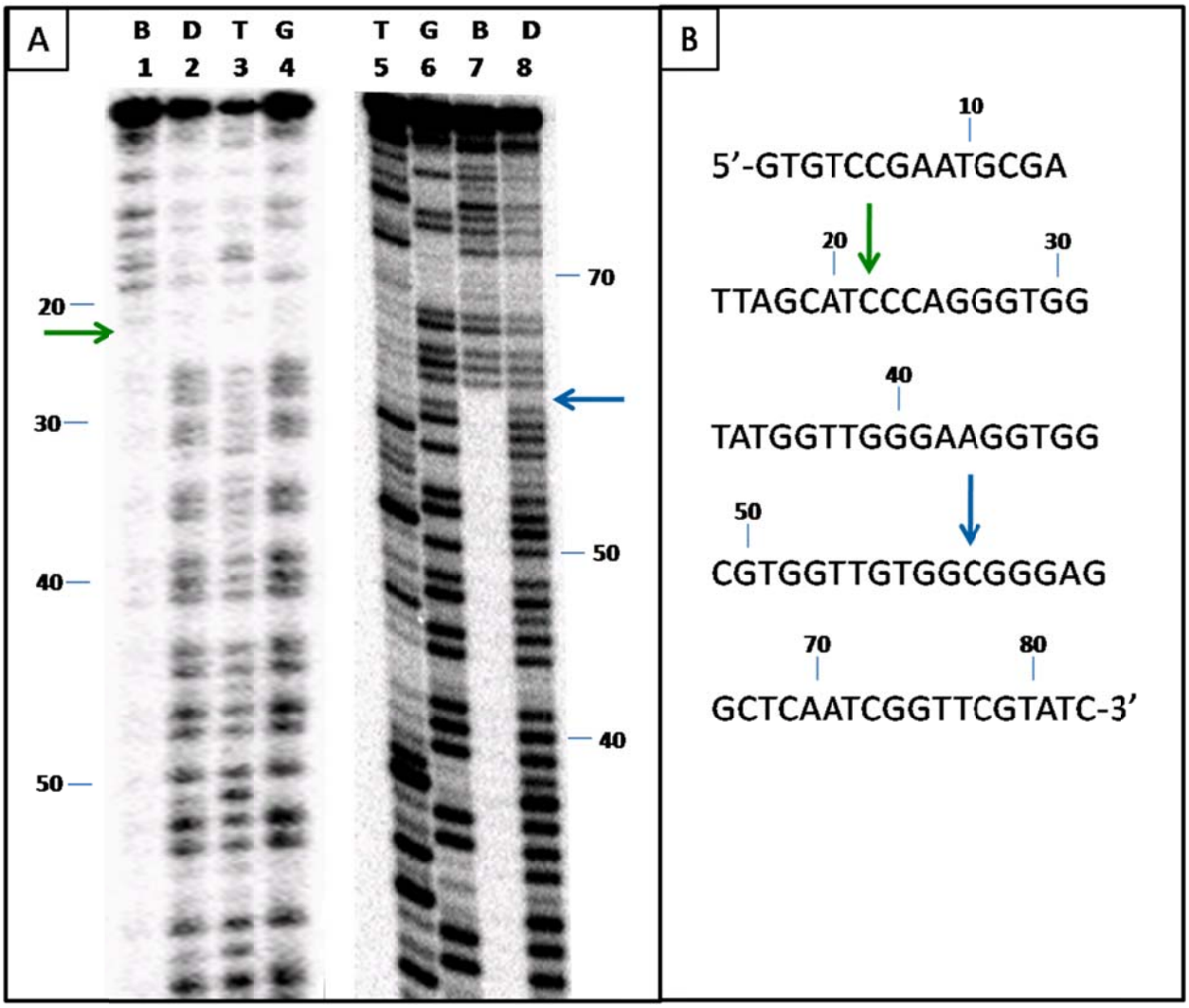

Figure S11: (A) Fragment binding experiments to map the boundaries of the clone 69 aptamer domain. Lanes G: G-specific cleavage ladder; lanes T: T-specific cleavage ladder; lanes B: mixture of G- and T-specific cleavage fragments that remained bound to CTAPIII beads after washing; lanes D: fragments decanted and washed from CTAPIII beads. Lanes 1-4: 3'-labelled fragments; lanes 5-8: 5'-labelled fragments. Fragments were resolved by 12% PAGE. **(B)** The blue and green arrows denote the first required nucleotide at the 3'- and 5'- ends, respectively, of the core aptamer domain.

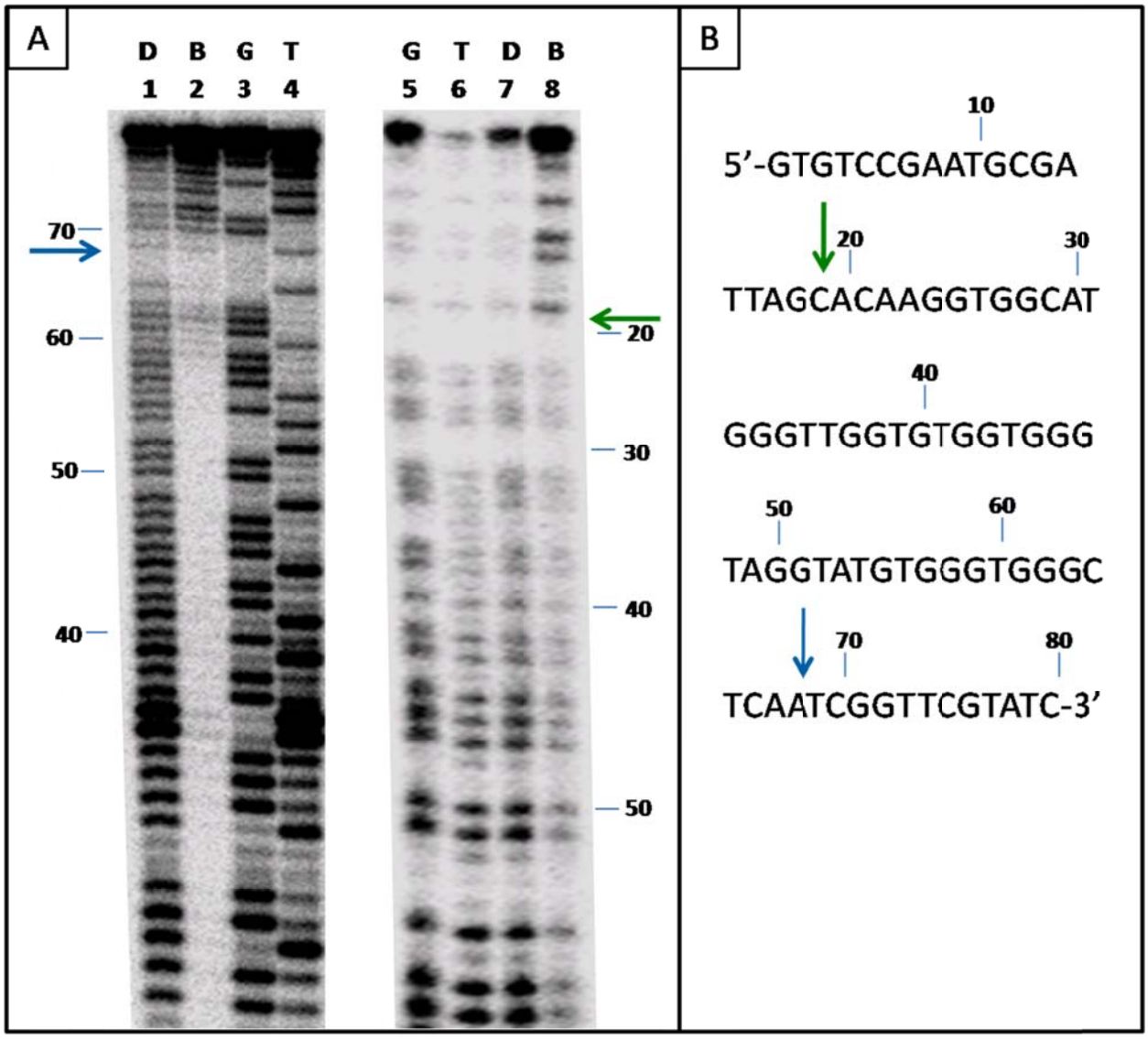

Figure S12: (A) Fragment binding experiments to map the boundaries of the clone 72 aptamer domain. Lanes G: G-specific cleavage ladder; lanes T: T-specific cleavage ladder; lanes B: mixture of G- and T-specific cleavage fragments that remained bound to CTAPIII beads after washing; lanes D: fragments decanted and washed from CTAPIII beads. Lanes 1-4: 5'-labelled fragments; lanes 5-8: 3'-labelled fragments. Fragments were resolved by 12% PAGE. **(B)** The blue and green arrows denote the first required nucleotide at the 3'- and 5'- ends, respectively, of the core aptamer domain.

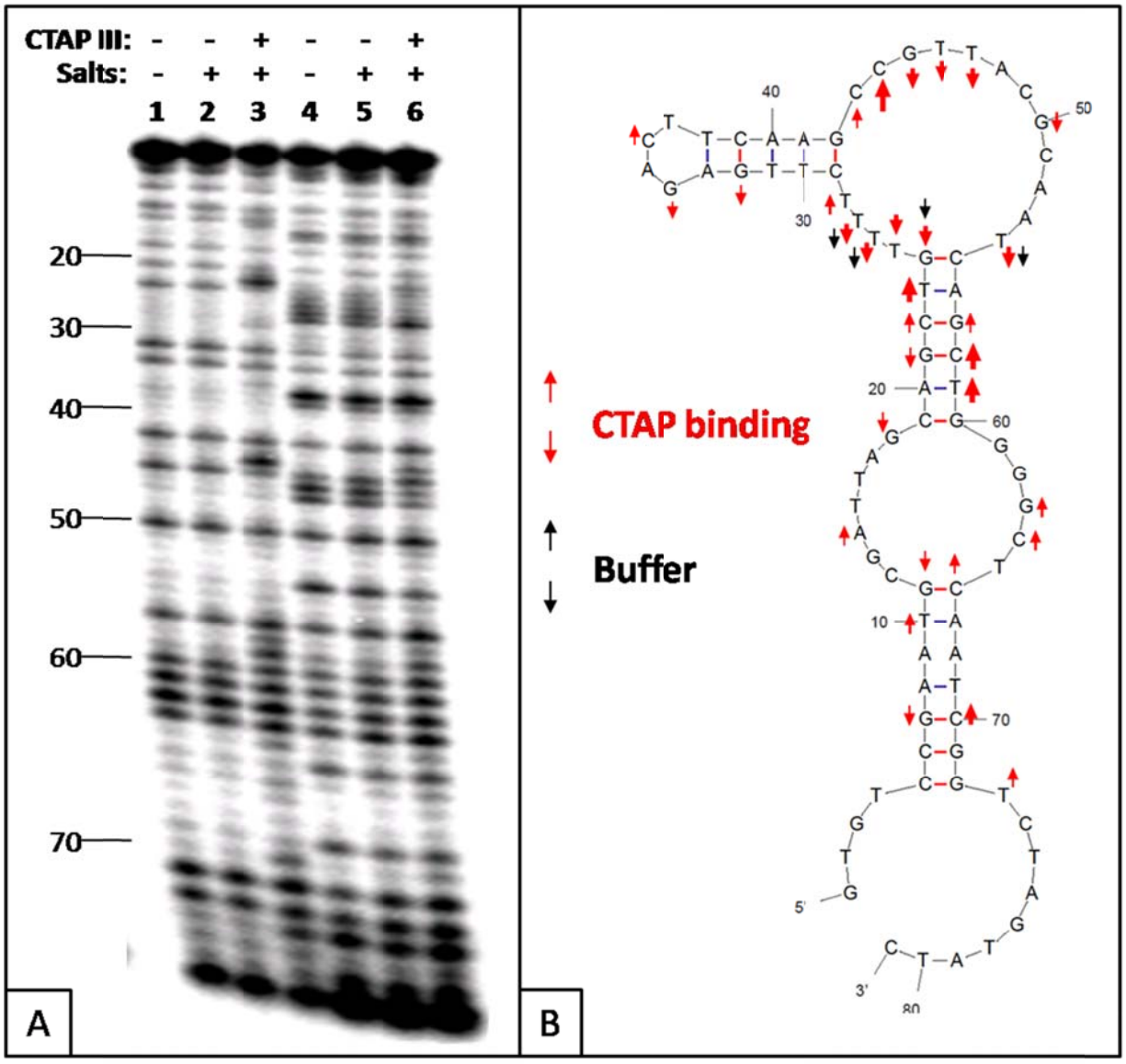

Figure S13: (A) DMS and $KMnO_4$ protection assays for 3`-^{32}P-labelled clone 69 analyzed by 12% denaturing PAGE. Lane 1: DMS treatment in TE buffer; lane 2: DMS treatment in binding buffer; lane 3: DMS treatment in binding buffer with CTAPIII; lane 4: $KMnO_4$ treatment in TE buffer; lane 5: $KMnO_4$ treatment in binding buffer; lane 6: $KMnO_4$ treatment in binding buffer with CTAPIII. **(B)** The degree of change in reactivity of G and C towards DMS and T towards $KMnO_4$ is approximated by the thickness of arrow.

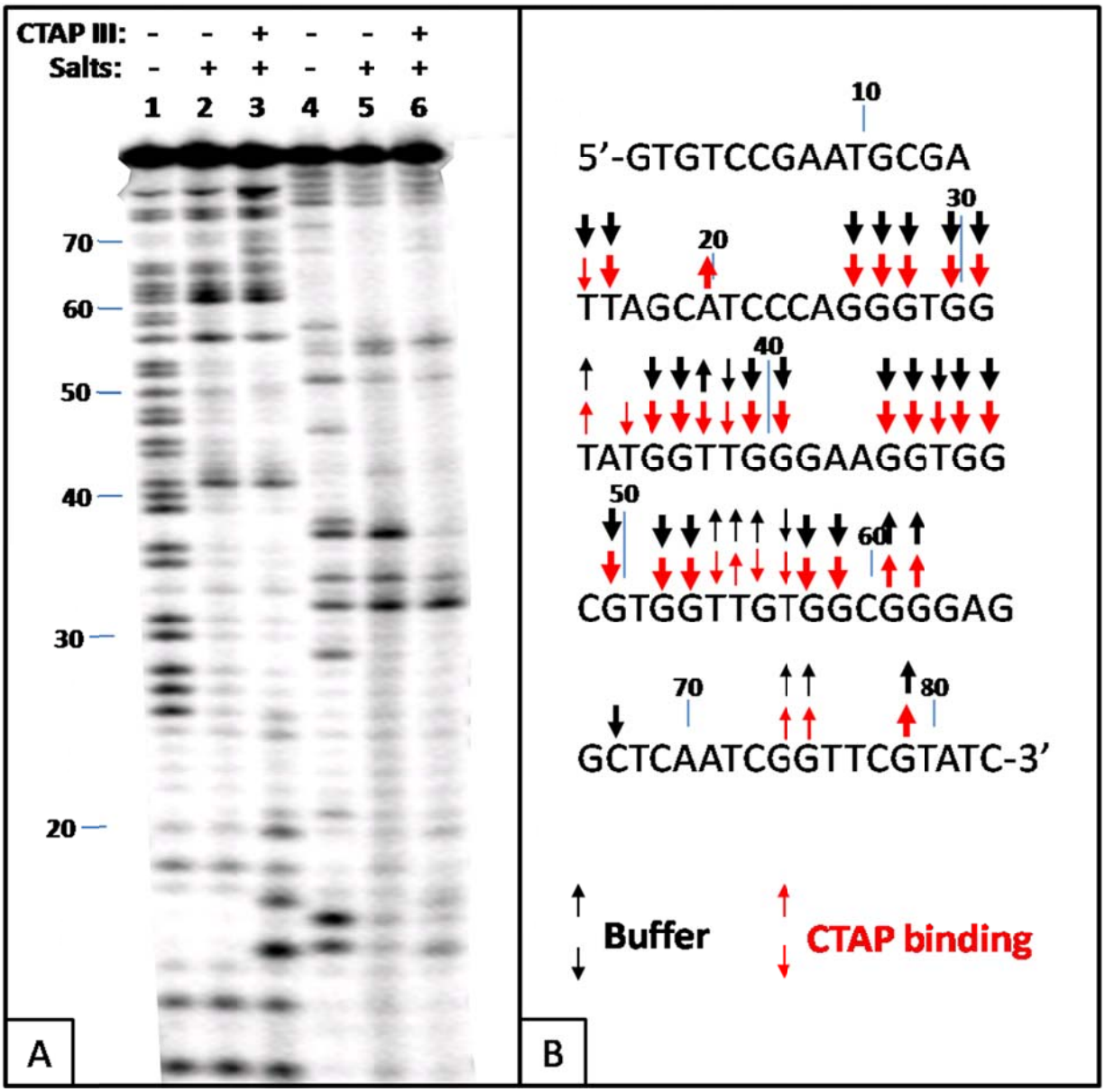

Figure S14: (A) DMS and $KMnO_4$ protection assays for 5`-^{32}P-labelled clone 69 analyzed by 12% denaturing PAGE. Lane 1: DMS treatment in TE buffer; lane 2: DMS treatment in binding buffer; lane 3: DMS treatment in binding buffer with CTAPIII; lane 4: $KMnO_4$ treatment in TE buffer; lane 5: $KMnO_4$ treatment in binding buffer; lane 6: $KMnO_4$ treatment in binding buffer with CTAPIII. **(B)** The degree of change in reactivity of G and C towards DMS and T towards $KMnO_4$ is approximated by the thickness of arrow.

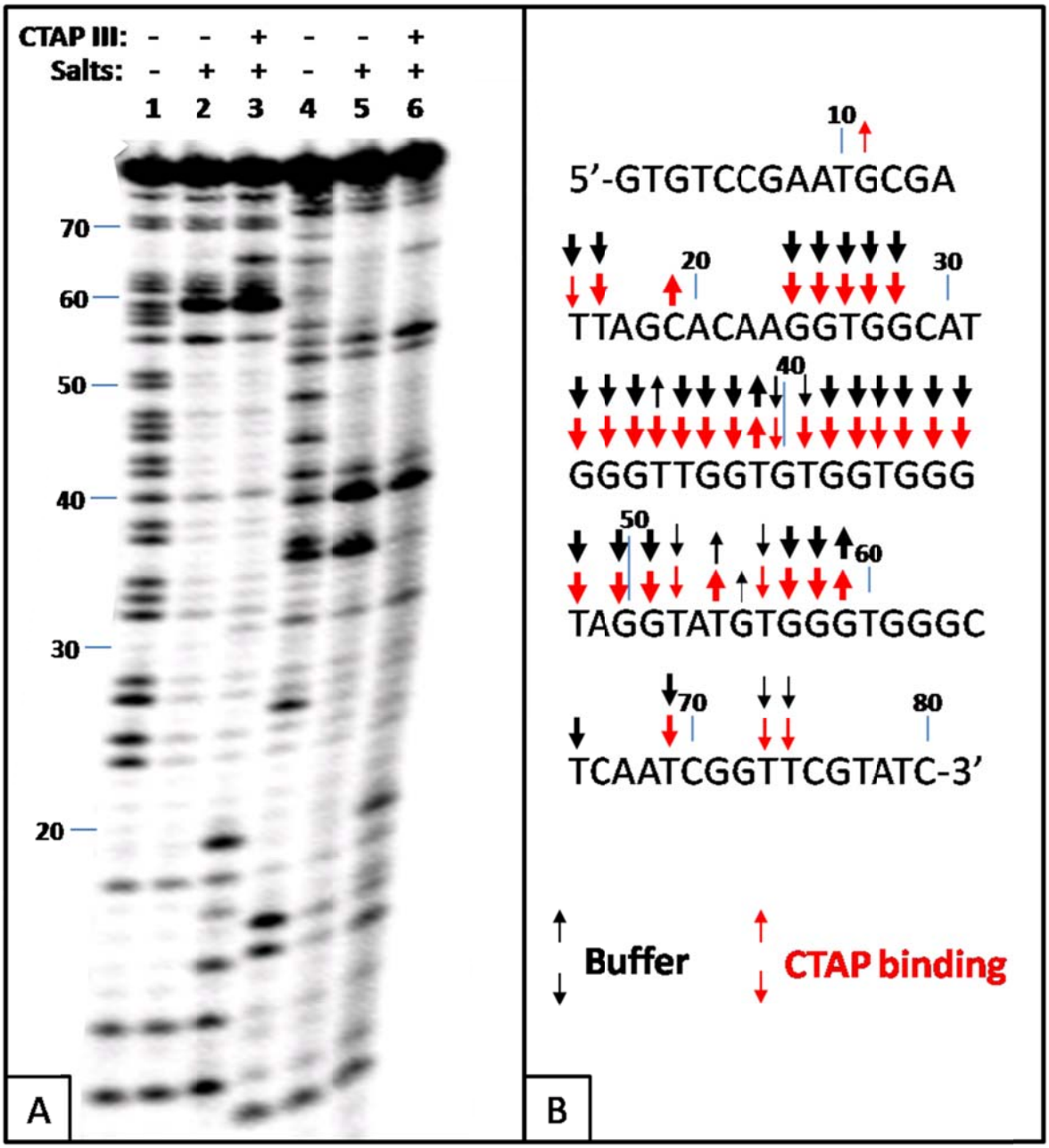

Figure S15: (A) DMS and $KMnO_4$ protection assays for 5`-^{32}P-labelled clone 72 analyzed by 12% denaturing PAGE. Lane 1: DMS treatment in TE buffer; lane 2: DMS treatment in binding buffer; lane 3: DMS treatment in binding buffer with CTAPIII; lane 4: $KMnO_4$ treatment in TE buffer; lane 5: $KMnO_4$ treatment in binding buffer; lane 6: $KMnO_4$ treatment in binding buffer with CTAPIII. **(B)** The degree of change in reactivity of G and C towards DMS and T towards $KMnO_4$ is approximated by the thickness of arrow.

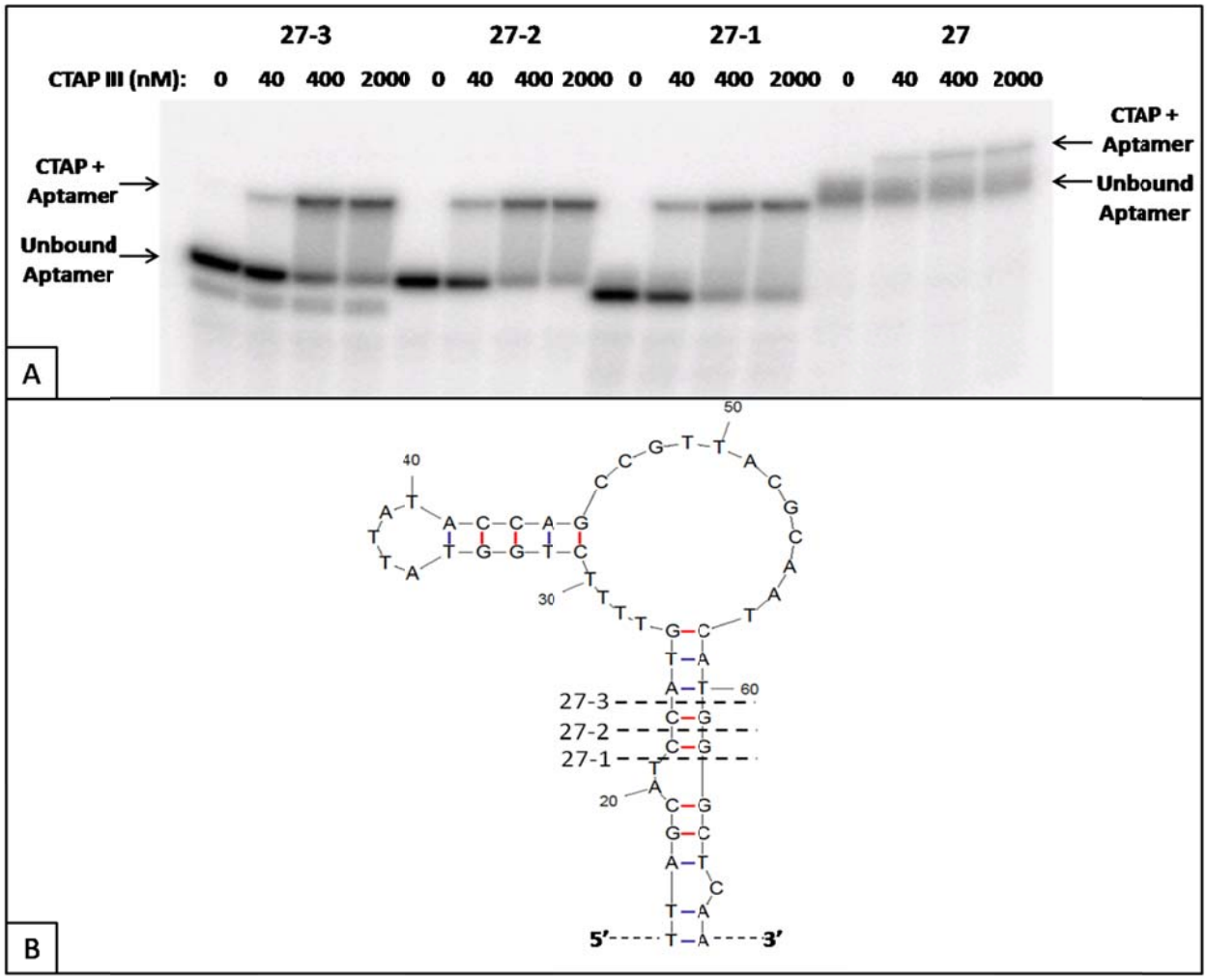

Figure S16: (**A**) Native gel analysis of CTAPIII binding by truncated versions of aptamer clone 27, as well as the full sequence isolated after SELEX. (**B**) The truncation sites are marked on the predicted secondary structure of clone 27.

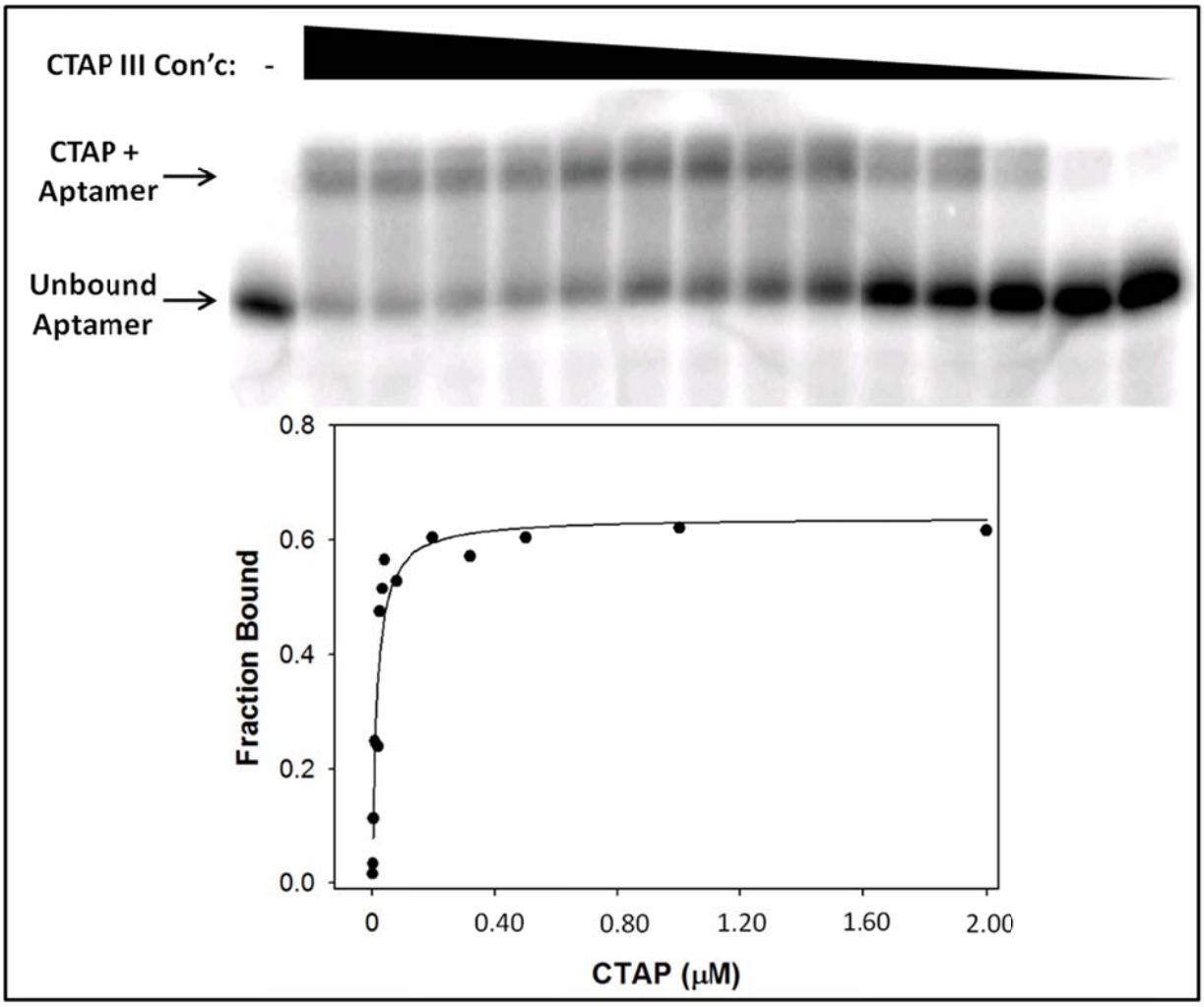

Figure S17: Measurement of the CTAPIII binding affinity of clone 27-1 by native gel electrophoretic mobility shift analysis. The fitted K_d value was 14 ± 3 nM.

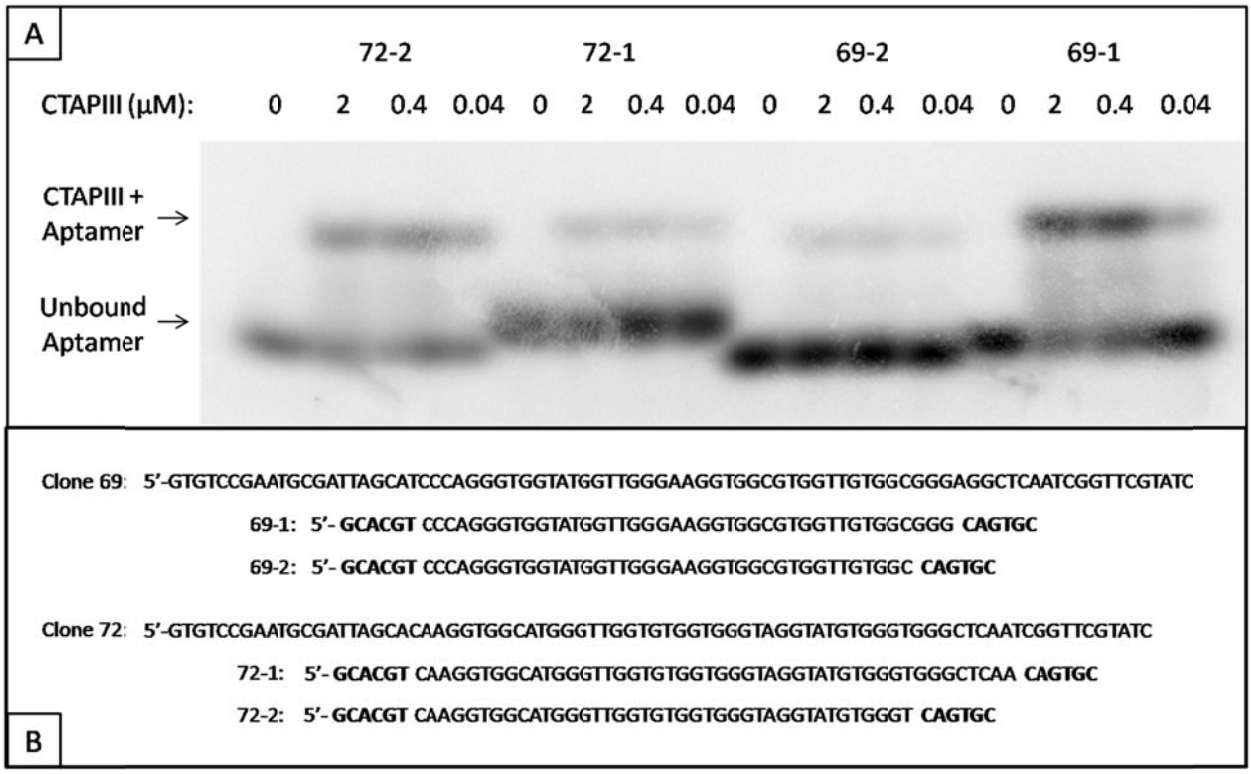

Figure S18: (A) Native gel analysis of CTAPIII binding by truncated versions of aptamer clones 69 and 72. **(B)** Alignment of the truncated and full length sequences. The bold sequences were added in an effort to introduce a base paired stem such that the aptamers could be attached to a sensor construct via a three-way helical junction.

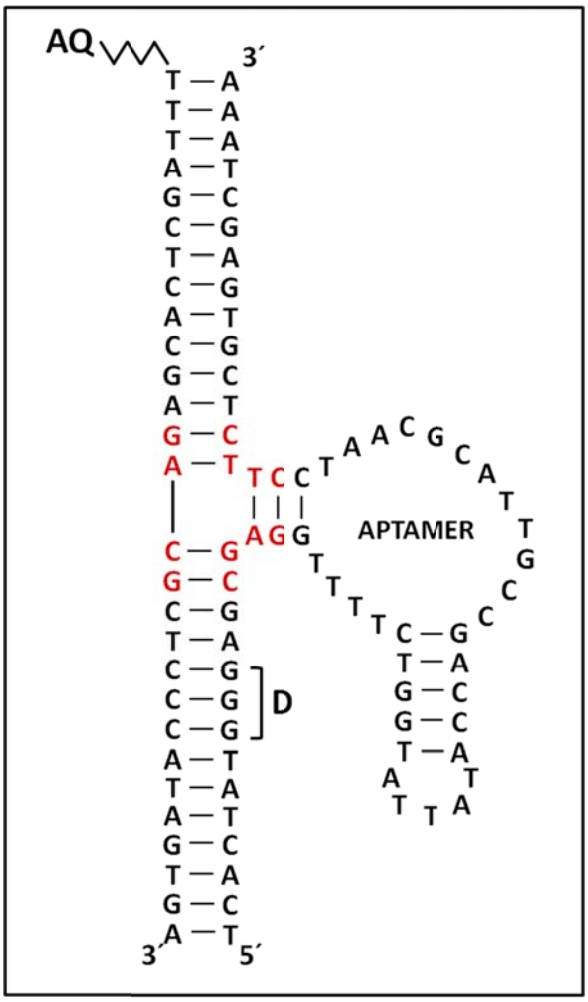

Figure S19: Secondary structure of CLD construct **S3**, which incorporates the clone 27-1 aptamer. The three-way junction is highlighted in red. Variations of the highlight junction sequence are shown in Figure S20. Oxidative damage to the distal guanine triplet (indicated by **D**) indicates charge transfer to the tethered AQ photo-oxidant.

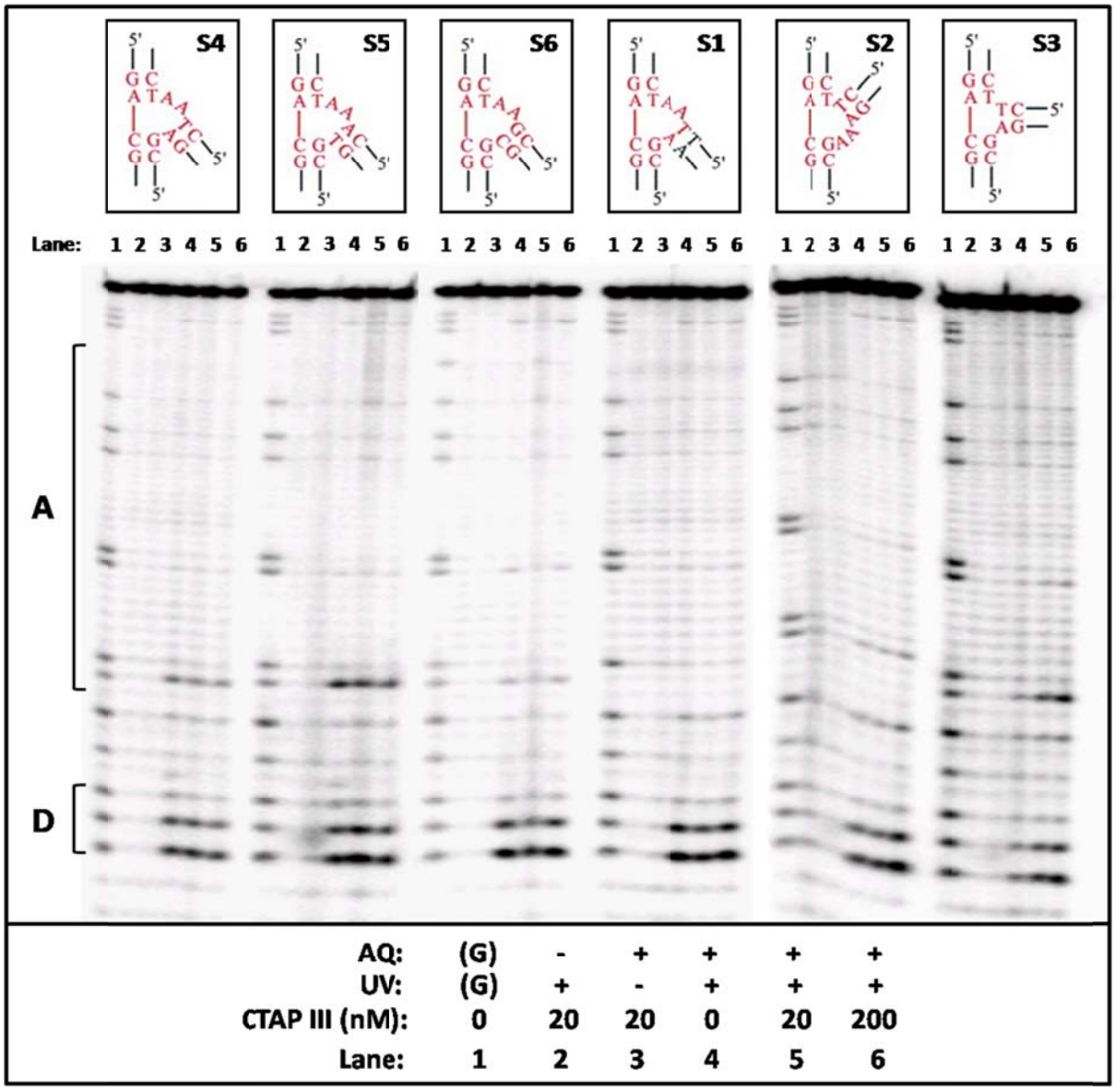

Figure S20: Biochemical charge transfer assay for the detection of CTAPIII by CLDs incorporating clone 27-1 with six different three-way junctions. Lanes 1: G-specific cleavage ladder; lanes 2: negative control lacking AQ; lanes 3: negative control lacking UV irradiation; lanes 4: sensor irradiation in the absence of CTAPIII; lanes 5: sensor irradiation in the presence of 20 nM CTAPIII; lanes 6: sensor irradiation in the presence of 200 nM CTAPIII.

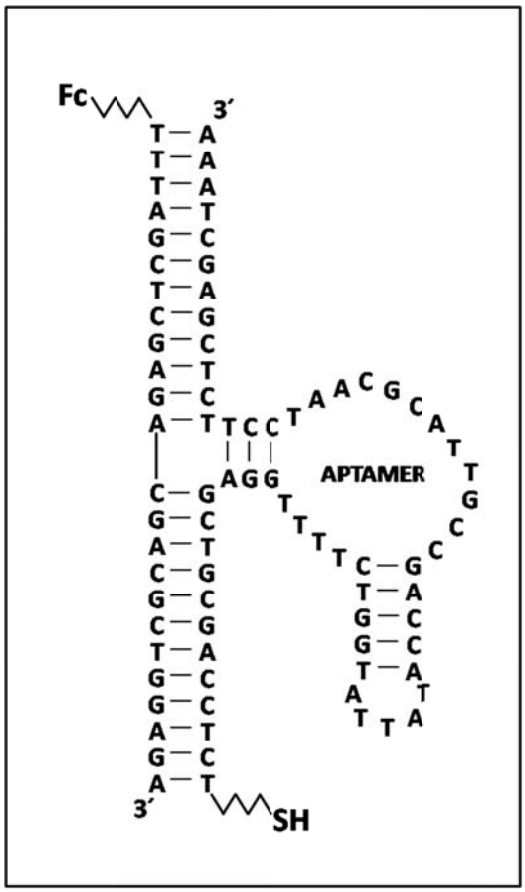

Figure S21: Predicted secondary structure for the **S3** CLD adapted for use in electrochemical measurements. The aptamer-containing strand is labelled at its 5'-terminus with a C6-thiol to allow immobilization on a gold electrode surface. The other strand is 5'-labelled with ferrocene carboxamide attached via a C6 linker. (Fc = ferrocene)

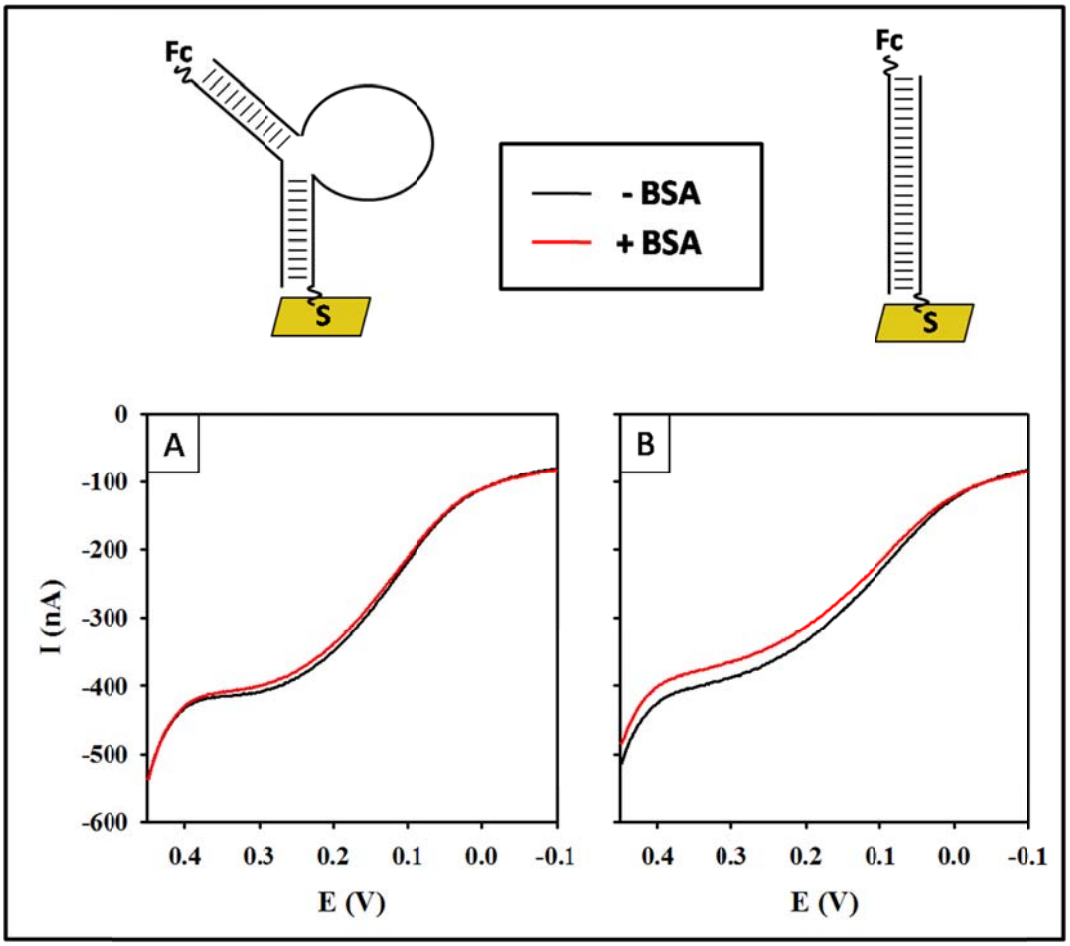

Figure S22: Square-wave voltammograms for **(A)** the **S3** CLD and **(B)** a fully complementary duplex DNA, each bound to a gold electrode via C6-thiol linker. The black and red voltammograms were collected with 0 nM and 100 nM BSA, respectively.

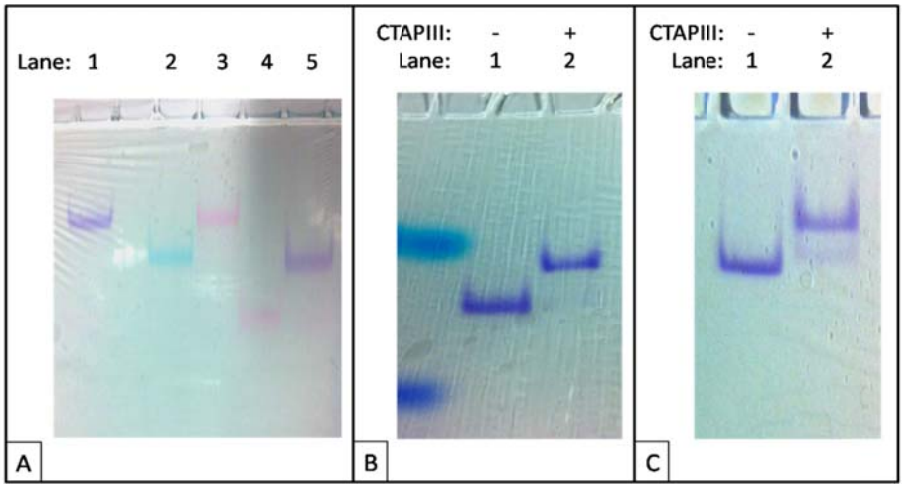

Figure S23: (A) Purification of annealed FRET constructs by 8% native PAGE (see Materials and Methods in the primary manuscript). Lane 1: annealed CLD **S3** construct terminally labelled with Cy3 and Cy5; Lane 2: Cy5 labelled CLD S3 oligonucleotide (not annealled to AQ-oligo); Lane 3: annealed CLD **S3** construct terminally labelled with Cy5 only; Lane 4: Cy3 labelled AQ-oligo; Lane 5: annealed 28-base pair duplex labelled with Cy3 and Cy5. **(B)** Confirmation, by electrophoretic mobility shift, that CTAPIII binds to CLD **S3** terminally labelled with Cy3 and Cy5. **(C)** Confirmation, by electrophoretic mobility shift, that CTAPIII binds to CLD **S3** terminally labelled with Cy3 and internally labelled with Cy5. Samples for electrophoretic mobility shift assays shown in panels (B) and (C) contained: 10 µM Cy5-labelled CLD **S3** oligo, 10 µM Cy3-labelled AQ-oligo, 50 mM Tris-HCl pH 8.0, 25 mM KCl, 1 mM $MgCl_2$. Samples were prepared with and without 30 µM CTAPIII.

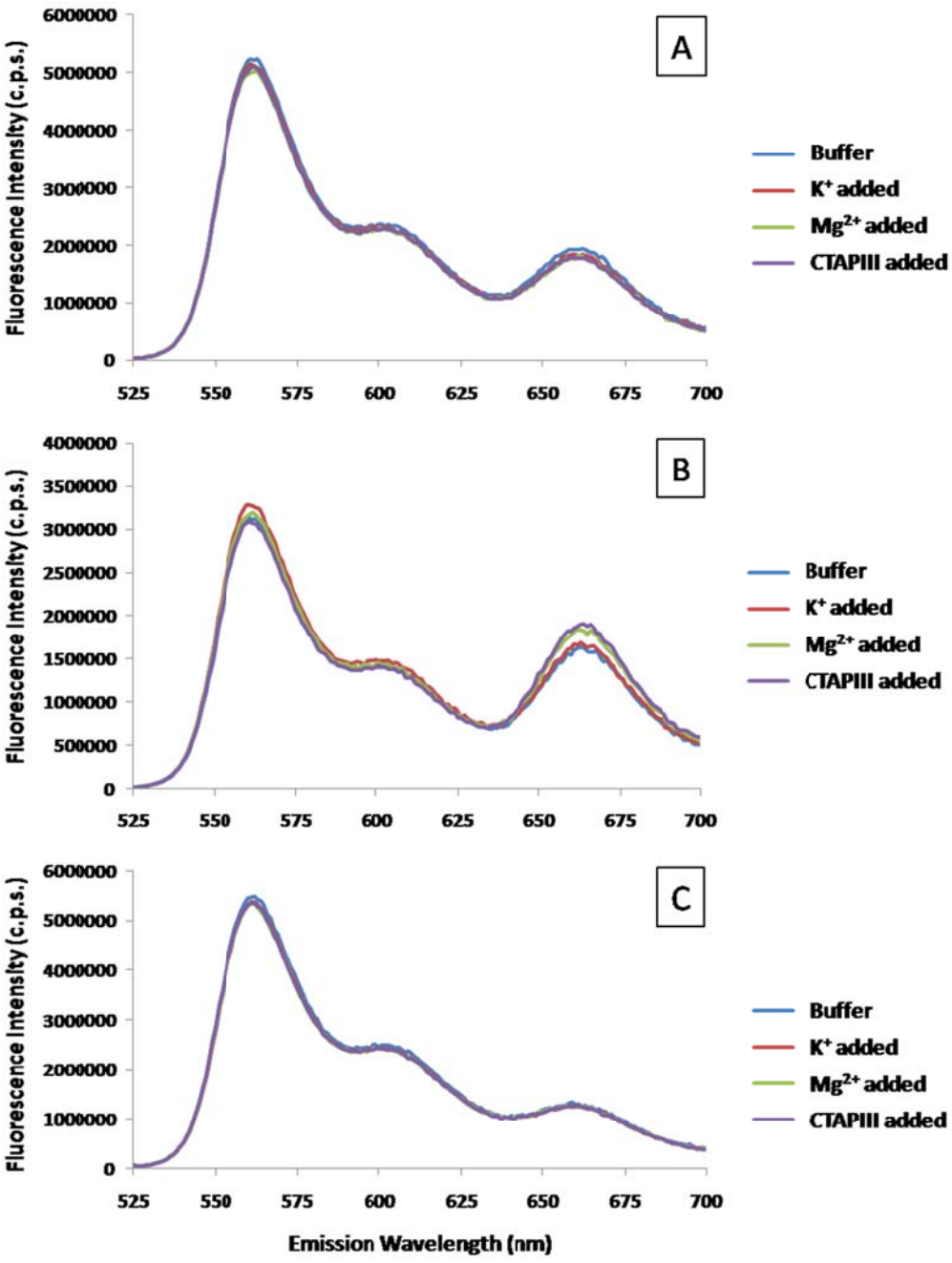

Figure S24: FRET emission spectra with Cy3 excitation at λ_{ex} = 513 nm for **(A)** CLD **S3** labelled with Cy3 and Cy5 at the termini of the reporter and detector stems, respectively. **(B)** CLD **S3** labelled with Cy3 at the terminus of the reporter stem and internally labelled with Cy5, within the aptamer domain at a non-conserved thymidine residue. **(C)** A 28-base pair duplex labelled at its termini with Cy3 and Cy5. See Figure 8 and the Materials and Methods in the primary manuscript for FRET sample oligonucleotide sequences.

References:

(s1) Proudfoot, A.E.I., Peitsch, M.C., Power, C.A., Allet, B., Mermod, J.-J., Bacon, K., Wells, T.N. *J. Prot. Chem.* **1997**, *16*, 37-49.

(s2) Malkowski, M.G., Wu, J.Y., Lazar, J.B., Johnson, P.H., Edwards, B.F.P. *J. Biol. Chem.* **1995**, *270*, 7077-7087.

(s3) Schagger, H. *Nat. Prot.* **1990**,*1*, 16-22.

(s4) Telser, J., Cruickshank, K.A., Morrison, L.E., Netzel, T.L., Chan, K. *J. Am. Chem. Soc.* **1989**, *111*, 7226-7232.

(s5) Fahlman, R.P., Sen, D. *J. Am. Chem.Soc.* **2002**, *124*, 4610-4616.

(s6) Yang, Y., Mayo, K.H., Daly, T.J., Barry, J.K., La Rosa, G.J. *J. Biol. Chem.* **1994**, *269*, 20110-20118.

(s7) a) Ellington, A.D. , Szostak, J.W. *Nature*, **1990**, *346*, 818-822; Tuerk, C., Gold, L. *Science*, **1990**, *249*, 505-510.